Atom localization and center-of-mass wave-function determination via multiple simultaneous quadrature measurements

Jörg Evers,[1,2,*] Shahid Qamar,[1,†] and M. Suhail Zubairy[1,3,4,‡]
[1]*Center for Quantum Physics, COMSATS Institute of Information Technology, G-5, Islamabad, Pakistan*
[2]*Max-Planck-Institut für Kernphysik, Saupfercheckweg 1, D-69117 Heidelberg, Germany*
[3]*Institute for Quantum Studies and Department of Physics, Texas A&M University, College Station, Texas 77843, USA*
[4]*Texas A&M University at Qatar, Education City, P.O. Box 23874, Doha, Qatar*
(Received 5 December 2006; published 8 May 2007)

We discuss localization and center-of-mass wave-function measurement of a quantum particle using multiple simultaneous dispersive interactions of the particle with different standing-wave fields. In particular, we consider objects with an internal structure consisting of a single ground state and several excited states. The transitions between ground and the corresponding excited states are coupled to the light fields in the dispersive limit, thus giving rise to a phase shift of the light field during the interaction. We show that multiple simultaneous measurements allow both an increase in the measurement or localization precision in a single direction and the performance of multidimensional measurements or localization. Further, we show that multiple measurements may relax the experimental requirements for each individual measurement.

DOI: 10.1103/PhysRevA.75.053809 PACS number(s): 42.50.Ct, 42.50.Vk, 03.75.Be, 03.65.Wj

I. INTRODUCTION

Initiated by the discussion on Heisenberg's famous microscope, precise spatial measurement of quantum objects has been a subject of considerable interest. In general, such measurements on quantum objects face problems similar to measurements on classical objects, for example, the diffraction limit. Due to the large range of applications of high-resolution microscopy, e.g., in biology, nanosciences, or chemistry, a number of approaches to imaging have been developed to overcome these limitations [1]. A particularly promising ansatz is near-field imaging, where the distance between object and measurement device is small enough that so-called evanescent electromagnetic waves originating from the object can be picked up by the microscope [2]. The requirement of a very small distance between object and imaging system, however, restricts the range of potential applications.

Somewhat complementary to these efforts, recently schemes have been developed which allow one to perform precision measurements on quantum objects in the far-field region. One approach is to modify the effective focal spot, e.g., by using interference of two overlapping light beams [3], or by selectively suppressing fluorescence from parts of the diffraction-limited focal spot, resulting in an effective focal spot smaller than predicted by Abbe's diffraction limit [4]. Another approach is to encode the desired spatial information in an observable that is not affected by the usual diffraction limitations [5–13]. For example, the interaction of the quantum particle with a standing-wave laser field has an interaction strength that depends on the position of the particle with respect to the nodes of the standing wave [5,6]. If an observable is chosen that depends on this interaction strength, then the position in the standing wave can be reconstructed from the measurement result. Apart from this near-resonant interaction between quantum particle and field, also nonresonant interaction can be used. For example, the phase shift on the standing-wave field due to a dispersive interaction with the quantum object can be measured to give spatial information [7–10].

The schemes that facilitate a spatially modulated light field as a reference for the position measurement, however, face a common problem. The far-field measurements typically only allow one to reconstruct the interaction strength between quantum object and field. But, due to the periodicity of the standing-wave intensity modulation, the mapping between coupling intensity and spatial position is not unique. Rather, there is a large number of potential positions within the standing-wave field that gives rise to equal coupling strength. Therefore, such measurements typically have to be accompanied by a conventional position measurement that allows one to pinpoint the position ideally to about $\lambda/2$, where λ is the wavelength of the incident light field. The far-field measurement then is used to refine this conventional position measurement to a small set of narrow potential positions within the classical range of $\lambda/2$.

To relax the requirement of an ideal conventional measurement, different approaches can be used. For example, sub-half-wavelength localization has been achieved by means of electromagnetically induced transparency in a more advanced control scheme [11]. Here, the potential positions from the localization measurement are restricted to one-half of each wavelength, and therefore allow for better localization with the same conventional measurement resolution. An alternative ansatz is to use multiple measurements. For example, in [12], the measurement of the atom-field interaction was combined with a Ramsey-type measurement on the internal state of the quantum particle. This gives rise to addi-

*Electronic address: joerg.evers@mpi-hd.mpg.de
†Permanent address: Department of Physics and Applied Mathematics, Pakistan Institute of Engineering and Applied Sciences, Nilore, Islamabad 45650, Pakistan. Electronic address: shahid_qamar@pieas.edu.pk
‡Electronic address: zubairy@physics.tamu.edu

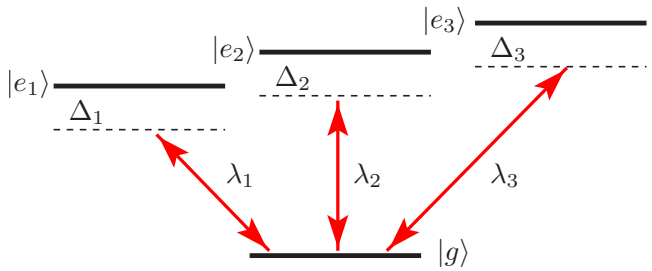

FIG. 1. (Color online) Internal structure of the quantum particle considered. λ_j $(j\in\{1,2,3\})$ are the coupling constants between transition and laser field; Δ_j are the detunings, which are considered large such that the interaction is dispersive.

tional interference effects which modulate the spatial probability distribution for the localization, but typically does not relax the requirements for the conventional measurement. Another approach is to apply a sequence of different measurements, e.g., by letting the atom pass several standing-wave fields [5,7–9]. This does allow one to improve the localization, but increases the total interaction time of atom and measurement fields. Furthermore, typical approximations used in the analysis, such as a negligible transverse velocity of the atom, become worse if several sequential measurements are applied. Finally, it is typically assumed that the quantum particle remains unchanged between the different measurements, which is questionable, in particular, if the atom is in an excited state.

To overcome these limitations, in this paper, we discuss setups that allow one to perform multiple *simultaneous* spatial measurements on a single quantum particle. In particular, we discuss the dispersive interaction of a quantum particle with several independent standing-wave field modes. The internal structure of the quantum particle is modeled as a four-level scheme with one ground state and three excited states, which for an atom could be Zeeman sublevels. Our analysis encompasses up to three simultaneous measurements, from a single spatial dimension up to three-dimensional position measurements. We show that both the localization and the measurement of the center-of-mass wave function of the particle can be improved by multiple simultaneous measurements. Finally, we show that multiple measurements may relax the experimental requirements for the individual measurements.

II. ANALYSIS

A. System Hamiltonian in the dispersive limit

We consider a four-level scheme with ground state $|g\rangle$ and three excited states $|e_j\rangle$ $(j\in\{1,2,3\})$ as the internal structure of the quantum particle (see Fig. 1). For example, for an atom, the ground state could be an S state (angular momentum $l=0$), and the excited states could be Zeeman sublevels of a P state $(l=1)$. In the following, we discuss this case of three independent fields coupling to the particle. Note that, since we work off-resonantly in the dispersive limit, the restriction to three transitions is meaningful since they can be distinguished by different polarizations of the laser fields. If

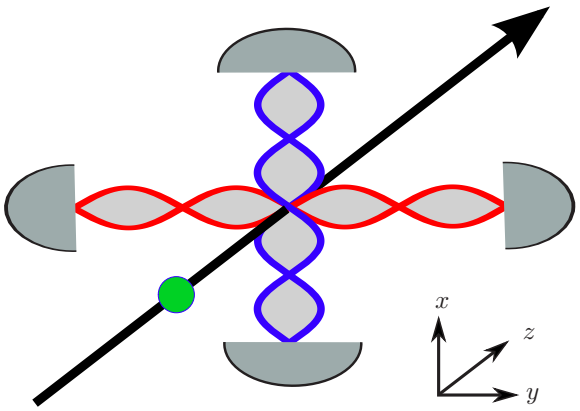

FIG. 2. (Color online) One of the setups discussed in this paper. Here, a quantum object flies through the intersection area of two cavity field modes. The cavity fields couple off-resonantly to different transitions between internal states of the quantum object and thus acquire a phase shift during the interaction due to its dispersive nature. Quadrature measurements of the cavity fields then allow a two-dimensional localization of the particle.

two of the transitions are to be driven by fields with equal polarization, then the frequencies of these two fields should be very different in order to treat the interactions independently. In this case, the generalization of our analysis to more than three transitions is straightforward. An example setup is shown in Fig. 2. In this example, two cavity fields are used for a two-dimensional localization of a quantum particle flying through the cavity field intersection area.

Each of the three dipole-allowed transitions is coupled to an individual cavity mode described by the creation and annihilation operators $a_j^\dagger, a_j$ $(j\in\{1,2,3\})$. The energy of the ground state is $\hbar\omega_g$, the excited state j has energy $\hbar\omega_j$, and the frequencies of the cavity fields are ν_j. The total Hamiltonian $H=H_{\rm at}+H_{\rm cav}+H_{\rm int}$ consists of the free atomic part $H_{\rm at}$, the free cavity field part $H_{\rm cav}$, and the interaction part $H_{\rm int}$ given by [14,15]

$$H_{\rm at}=\hbar\omega_g|g\rangle\langle g|+\sum_{j=1}^{3}\hbar\omega_j|e_j\rangle\langle e_j|, \tag{1}$$

$$H_{\rm cav}=\sum_{j=1}^{3}\hbar\nu_j a_j^\dagger a_j, \tag{2}$$

$$H_{\rm int}=\sum_{j=1}^{3}\hbar(\lambda_j a_j|e_j\rangle\langle g|+\lambda_j^* a_j^\dagger|g\rangle\langle e_j|). \tag{3}$$

In the dispersive limit, the applied laser fields do not transfer population between the atomic states due to the large laser field detunings. Rather, they induce a phase shift on the involved states [5,7,8,16–19]. In the following, we adopt the method of unitary transformation introduced in [19] to obtain the effective Hamiltonian describing the dispersive atom-field interaction. To this end, we define the following unitary transformation of an operator X, which effectively decouples the excited states from the ground state in the dispersive limit:

$$X \to e^{S} X e^{-S}, \tag{4}$$

where

$$S = \sum_{j=1}^{3} \frac{-1}{\Delta_j} (\lambda_j a_j \sigma_{e_j g} - \lambda_j^* a_j^\dagger \sigma_{g e_j}). \tag{5}$$

We have introduced the detunings $\Delta_j = \nu_j - (\omega_j - \omega_g)$. Applying this transformation to the Hamiltonian Eqs. (1)–(3), and expanding up to second order in the coupling constants, the transformed Hamiltonian $\bar{H}$ evaluates to

$$\bar{H} = H_{\rm at} + H_{\rm cav} + H_{\rm shift} + H_{\rm c}, \tag{6}$$

$$H_{\rm shift} = -\sum_{j=1}^{3} \hbar \frac{|\lambda_j|^2}{\Delta_j} \sigma_{e_j e_j} (a_j^\dagger a_j + 1) + \sum_{j=1}^{3} \hbar \frac{|\lambda_j|^2}{\Delta_j} \sigma_{gg} a_j^\dagger a_j, \tag{7}$$

$$\begin{aligned} H_{\rm c} = &-\left[\hbar \frac{\lambda_1 \lambda_2^*}{2} \left(\frac{1}{\Delta_1} + \frac{1}{\Delta_2}\right) a_2^\dagger a_1 \sigma_{e_1 e_2} + \text{H.c.}\right] \\ &-\left[\hbar \frac{\lambda_1 \lambda_3^*}{2} \left(\frac{1}{\Delta_1} + \frac{1}{\Delta_3}\right) a_3^\dagger a_1 \sigma_{e_1 e_3} + \text{H.c.}\right] \\ &-\left[\hbar \frac{\lambda_2 \lambda_3^*}{2} \left(\frac{1}{\Delta_2} + \frac{1}{\Delta_3}\right) a_3^\dagger a_2 \sigma_{e_2 e_3} + \text{H.c.}\right]. \end{aligned} \tag{8}$$

Note that the phase shifts in Eq. (7) are consistent with results obtained from second-order perturbation theory. For example, the energy shift of the ground state $|g, n_1, n_2, n_3\rangle$ with energy $E_0 = \hbar(\omega_g + \Sigma_{j=1}^3 n_n \nu_n)$ and n_j photons in laser field mode j, respectively, can be evaluated using second-order perturbation theory to give

$$\left\langle g, n_1, n_2, n_3 \middle| H_{\rm int} \frac{1}{E_0 - H} H_{\rm int} \middle| g, n_1, n_2, n_3 \right\rangle = \hbar \sum_{j=1}^{3} \frac{|\lambda_j|^2}{\Delta_j} n_j. \tag{9}$$

Similarly, the perturbation for an initially excited state $|e_i\rangle$ evaluates to

$$\left\langle e_i, n_1, n_2, n_3 \middle| H_{\rm int} \frac{1}{E_0 - H} H_{\rm int} \middle| e_i, n_1, n_2, n_3 \right\rangle = -\hbar \frac{|\lambda_i|^2}{\Delta_i} (n_i + 1), \tag{10}$$

where the additional constant shift $-\hbar|\lambda_i|^2/\Delta_i$ is the spontaneous energy shift due to the vacuum.

Further, it can be seen from Eq. (8) that, as compared to the case of a single transition, in general there are additional terms, which correspond to a coupling of the upper states via the cavity modes. Depending on the atomic state, these will modify the internal dynamics.

If one assumes large detunings Δ_j in the dispersive limit and that the atom initially is in the ground state $|g\rangle$, then $\bar{H}$ reduces to a much simpler effective Hamiltonian given by

$$\hat{H} = \hbar \omega_g \sigma_{gg} + H_{\rm cav} + \sum_{j=1}^{3} \hbar \frac{|\lambda_j|^2}{\Delta_j} \sigma_{gg} a_j^\dagger a_j. \tag{11}$$

Thus, the unitary transformation Eq. (4) has effectively decoupled the excited states from the dynamics as desired. In a suitable rotating frame, this Hamiltonian, which will be used in the further analysis, reads

$$V = \sum_{j=1}^{3} \hbar \frac{|\lambda_j|^2}{\Delta_j} \sigma_{gg} a_j^\dagger a_j. \tag{12}$$

B. Atom-field interactions

We now turn to the time evolution of the combined atom-field system under the influence of the interaction Hamiltonian Eq. (12). For this, we assume the initial state to be

$$\begin{aligned} |\Psi(t=0)\rangle = |g, \alpha, \beta, \gamma\rangle = e^{-(|\alpha|^2 + |\beta|^2 + |\gamma|^2)/2} \\ \times \sum_{l,m,n=0}^{\infty} \frac{\alpha^l \beta^m \gamma^n}{\sqrt{l!m!n!}} |g, l, m, n\rangle, \end{aligned} \tag{13}$$

which denotes a state where the atom is in the ground state $|g\rangle$, and the three cavity fields are in coherent states $|\alpha\rangle, |\beta\rangle, |\gamma\rangle$, respectively. Applying the time evolution operator under Hamiltonian Eq. (12)

$$U(0,t) = e^{-(i/\hbar)Vt} \tag{14}$$

then yields

$$|\Psi(t)\rangle = |g, \alpha e^{i\phi_1 t}, \beta e^{i\phi_2 t}, \gamma e^{i\phi_3 t}\rangle, \tag{15}$$

where

$$\phi_j = -\frac{|\lambda_j|^2}{\Delta_j} = -\frac{|\lambda_j^0|^2}{\Delta_j} \cos^2(k_j x + \xi_j). \tag{16}$$

Here and in the following, for the sake of notational simplicity, we specialize the analysis to localization in the x direction. The generalization to the multidimensional case is straightforward. A result of the form Eq. (16) can only be expected if the atom initially is in the ground state, and, due to the dispersive nature of the interaction, remains in the state throughout the whole evolution. In this case, the additional terms in the Hamiltonian Eq. (8) which couple the different upper states with each other do not contribute, and thus the time evolutions of the three field phases are independent.

Starting from these results, two routes to fix the actual phase shifts are possible. First, one may derive the total phase shift when the particle flies through a Gaussian intensity distribution with a certain speed and a certain width of the field mode. Second, one may assume as in [7] that the parameters are such that the maximum phase shifts $\phi_j t$ occurring if the particle flies through an antinode is π. This involves an appropriate choice of field strengths according to the particle velocity, and is favorable since it represents the optimum choice in terms of localization. Thus in the following we choose this latter option.

C. Field quadrature measurements

In this section, we focus on the spatial properties of the wave function. For this, note that the coupling constants λ_j are position dependent in the standing-wave field:

$$\lambda_j = \lambda_j^0 \cos(k_j x + \xi_j). \tag{17}$$

Here, k_j is the wave number of the field in cavity j, and ξ_j is the phase of the standing-wave field. Thus, the phase shift acquired by a particle passing through the standing wave depends on the position. We assume the particle wave function to be a pure state,

$$|\Psi(0)\rangle = \int dx\, g(x)|x,g\rangle, \tag{18}$$

where $g(x)$ is the normalized spatial center-of-mass amplitude of the particle. This ensures that the measurement of the phase shift of the cavity fields can be interpreted as a quantum localization, or collapse of the wave function. The internal state is chosen as the ground state $|g\rangle$. The time-dependent total wave function for internal and external degrees of freedom of the particle, as well as the field states is thus given by

$$|\Psi(t)\rangle = \int dx\, g(x) e^{-(i/\hbar)Vt}|x,g,\alpha,\beta,\gamma\rangle. \tag{19}$$

Using Eq. (15), this can be evaluated to give

$$|\Psi(t)\rangle = \int dx\, g(x)|x,g,\alpha e^{i\phi_1 t},\beta e^{i\phi_2 t},\gamma e^{i\phi_3 t}\rangle, \tag{20}$$

where each of the phases ϕ_i depends on the position of the particle in the corresponding cavities; see Eq. (16). We assume now that the particle has passed through the cavity, and perform a quadrature measurement on the fields. The measurement is characterized by the angle θ_j in the Wigner plane. For example, $\theta_j=0$ corresponds to the amplitude quadrature, whereas $\theta_j=\pi/2$ denotes the phase quadrature. Suppose the outcome of the measurement of field $|\alpha\rangle$ with angle θ_1 is the field quadrature state $|\chi_{\theta_1}^{\alpha}\rangle$. Then the state of the system after this measurement is given by

$$|\Psi(t)\rangle = N_\alpha \int dx\, g(x)\langle\chi_{\theta_1}^{\alpha}|\alpha e^{i\phi_1 t}\rangle|x,g,\beta e^{i\phi_2 t},\gamma e^{i\phi_3 t}\rangle, \tag{21}$$

where N_α is a normalization constant. One should note here that we have chosen the coherent field modes such that their polarizations are mutually orthogonal, so that they can be measured individually, and such that the corresponding creation and annihilation operators commute. Similarly, a measurement of the other two field modes with angles θ_2,θ_3 and results $|\chi_{\theta_2}^{\beta}\rangle,|\chi_{\theta_3}^{\gamma}\rangle$ finally creates a state

$$|\Psi(t)\rangle = N \int dx\, g(x)\langle\chi_{\theta_1}^{\alpha}|\alpha e^{i\phi_1 t}\rangle \times \langle\chi_{\theta_2}^{\beta}|\beta e^{i\phi_2 t}\rangle\langle\chi_{\theta_3}^{\gamma}|\gamma e^{i\phi_3 t}\rangle|x,g\rangle, \tag{22}$$

with overall normalization $N=N_\alpha N_\beta N_\gamma$. The probability amplitude distribution for the position of the particle in the x direction after the three measurements thus is

$$\Psi(x,t) = \langle x,g|\Psi(t)\rangle = Ng(x)\langle\chi_{\theta_1}^{\alpha}|\alpha e^{i\phi_1 t}\rangle\langle\chi_{\theta_2}^{\beta}|\beta e^{i\phi_2 t}\rangle \times \langle\chi_{\theta_3}^{\gamma}|\gamma e^{i\phi_3 t}\rangle. \tag{23}$$

From this, the conditional probability for the particle to be at position x given that the three field measurements had the results $|\chi_{\theta_1}^{\alpha}\rangle,|\chi_{\theta_2}^{\beta}\rangle,|\chi_{\theta_3}^{\gamma}\rangle$ can be written as

$$P(x|\chi_{\theta_1}^{\alpha},\chi_{\theta_2}^{\beta},\chi_{\theta_3}^{\gamma}) = |\Psi(x,t)|^2 = N^2|g(x)|^2 \times |\langle\chi_{\theta_1}^{\alpha}|\alpha e^{i\phi_1 t}\rangle|^2|\langle\chi_{\theta_2}^{\beta}|\beta e^{i\phi_2 t}\rangle|^2|\langle\chi_{\theta_3}^{\gamma}|\gamma e^{i\phi_3 t}\rangle|^2. \tag{24}$$

In this sense, the three measurements can be seen as independent, even though each of the three field phases is correlated with the position of the particle. The expression (24) also confirms the intuitive picture one may have from the setup, namely, that each of the three fields acquires an independent phase shift, which determines a set of potential positions of the particle. The true position of the atom is then bound to the intersection of these three possible sets.

We now proceed by evaluating the overlap integral of the coherent field states in the cavities with the measured quadrature field eigenstate. For this, we make use of the explicit expression [7]

$$|\chi_\theta\rangle = (2\pi)^{-1/4} e^{-(a^\dagger e^{i\theta} - \chi_\theta)^2/2 + \chi_\theta^2/4}|\mathrm{vac}\rangle, \tag{25}$$

where $|\mathrm{vac}\rangle$ denotes the vacuum state with zero photons in the cavity mode. We obtain, using $a|\alpha\rangle=\alpha|\alpha\rangle$,

$$\begin{aligned} A_\alpha(\chi_\theta|x) &= \langle\chi_\theta|\alpha e^{i\phi_1 t}\rangle \\ &= \frac{1}{\sqrt[4]{2\pi}}\langle\mathrm{vac}|e^{-(\alpha e^{i(\phi_1 t-\theta)} - \chi_\theta)^2/2 + \chi_\theta/4}|\alpha e^{i\phi_1 t}\rangle \\ &= \frac{1}{\sqrt[4]{2\pi}} e^{-(\alpha e^{i(\phi_1 t-\theta)} - \chi_\theta)^2/2 + \chi_\theta/4} e^{-|\alpha|^2/2}, \end{aligned} \tag{26}$$

and thus

$$P_\alpha(\chi_\theta|x) = |\langle\chi_\theta|\alpha e^{i\phi_1 t}\rangle|^2 = \frac{1}{\sqrt{2\pi}} e^{-2(\alpha_R - \chi_\theta/2)^2}, \tag{27}$$

where

$$\alpha_R = \mathrm{Re}(\alpha e^{i(\phi_1 t-\theta)}). \tag{28}$$

Similarly, the overlap integrals and probabilities $P_\beta(\chi_\theta|x), P_\gamma(\chi_\theta|x)$ corresponding to the other two cavity field modes can be evaluated.

D. Conditional probability

We now analyze the conditional probability Eq. (27) with the aim of identifying particle positions with maximum probability for a given measurement result χ_θ, or vice versa. For this, we differentiate with respect to the position x and obtain as necessary condition for extrema

$$0 = \frac{d}{dx}P_\alpha(\chi_\theta|x) = \frac{-4}{\sqrt{2\pi}}e^{-2(\alpha_R-\chi_\theta/2)^2}\left(\alpha_R - \frac{1}{2}\chi_\theta\right)\frac{d}{dx}\alpha_R$$

$$= -4P_\alpha(\chi_\theta|x)\left(\alpha_R - \frac{1}{2}\chi_\theta\right)\frac{d}{dx}\alpha_R, \tag{29}$$

which, since $P_\alpha(\chi_\theta|x) > 0$, splits into two cases

$$0 = \left(\alpha_R - \frac{1}{2}\chi_\theta\right), \tag{30a}$$

$$0 = \frac{d}{dx}\alpha_R. \tag{30b}$$

We also need to evaluate the second derivative in order to distinguish minima and maxima, and obtain

$$\frac{d^2}{dx^2}P_\alpha(\chi_\theta|x) = -4\left[P'_\alpha(\chi_\theta|x)\left(\alpha_R - \frac{1}{2}\chi_\theta\right)\alpha'_R + P_\alpha(\chi_\theta|x)(\alpha'_R)^2 + P_\alpha(\chi_\theta|x)\left(\alpha_R - \frac{1}{2}\chi_\theta\right)\alpha''_R\right], \tag{31}$$

where a prime denotes differentiation with respect to x.

We proceed with the first case Eq. (30a). Writing it out explicitly yields

$$\cos[\pi\cos^2(k_i x + \xi_i) - \theta] = \frac{\chi_\theta}{2\alpha}. \tag{32}$$

Therefore, this root occurs only if $|\chi_\theta/(2\alpha)| \leqslant 1$. We denote x values that satisfy Eq. (32) by $x^{(1)}_{\max}$. For any of these $x^{(1)}_{\max}$ values, one obtains for the conditional probability

$$P_\alpha(\chi_\theta|x^{(1)}_{\max}) = \frac{1}{\sqrt{2\pi}}, \tag{33}$$

which is the maximum possible probability. Thus, a further analysis in terms of minima or maxima of $P_\alpha(\chi_\theta|x)$ is not required in this case.

The second case Eq. (30b) in explicit form is

$$0 = \pi\alpha k_i \sin[\pi\cos^2(k_i x + \xi_i) - \theta]\sin[2(k_j x + \xi_i)]. \tag{34}$$

Again, there are two nontrivial possibilities,

$$0 = \sin[\pi\cos^2(k_i x + \xi_i) - \theta], \tag{35a}$$

$$0 = \sin[2(k_j x + \xi_i)]. \tag{35b}$$

Note that the two conditions Eqs. (35a) and (35b) are equivalent for $\theta = 0$.

The first condition Eq. (35a) is satisfied if $\pi\cos^2(k_i x + \xi_i) - \theta = n\pi$, where n is an integer number. Then, $\alpha_R = (-1)^n\alpha$. We denote the x satisfying this equation by $x^{(2a)}_{\text{ext}}$, since it is not clear yet whether there is a minimum or a maximum. The second derivative evaluates to

$$\frac{d^2}{dx^2}P_\alpha(\chi_\theta|x^{(2a)}_{\text{ext}}) = -4P_\alpha(\chi_\theta|x^{(2a)}_{\text{ext}})\left((-1)^n\alpha - \frac{1}{2}\chi_\theta\right)\alpha''_R$$

$$= 4\alpha k_j^2\pi^2 P_\alpha(\chi_\theta|x^{(2a)}_{\text{ext}})\sin^2[2(k_j x^{(2a)}_{\text{ext}} + \xi_j)] \times \left(\alpha - \frac{(-1)^n}{2}\chi_\theta\right). \tag{36}$$

The second derivative needs to be negative for $x^{(2a)}_{\text{ext}}$ to be a maximum, and this is only possible if $(-1)^n\chi_\theta > 2\alpha$. We denote these maxima by $x^{(2a)}_{\max}$. The probability for the extrema $x^{(2a)}_{\text{ext}}$ evaluates to

$$P_\alpha(\chi_\theta|x^{(2a)}_{\text{ext}}) = \frac{1}{\sqrt{2\pi}}e^{-2\{\alpha - [(-1)^n/2]\chi_\theta\}^2}, \tag{37}$$

which is smaller than $1/\sqrt{2\pi}$ for all maxima $x^{(2a)}_{\max}$ since then $(-1)^n\chi_\theta > 2\alpha$.

The second condition Eq. (35b) is satisfied if $(k_j x + \xi_i) = n\pi/2$, and the x are denoted by $x^{(2b)}_{\text{ext}}$. Then, $\alpha_R = (-1)^{n+1}\alpha\cos$, and

$$\frac{d^2}{dx^2}P_\alpha(\chi_\theta|x^{(2b)}_{\text{ext}}) = 4P_\alpha(\chi_\theta|x^{(2b)}_{\text{ext}})\left((-1)^n\alpha\cos\theta + \frac{1}{2}\chi_\theta\right)\alpha''_R$$

$$= 8\alpha k_j^2\pi P_\alpha(\chi_\theta|x^{(2b)}_{\text{ext}})\sin\theta\left((-1)^n\alpha\cos\theta + \frac{1}{2}\chi_\theta\right). \tag{38}$$

The complete discussion to separate the maximum values $x^{(2b)}_{\max}$ out of the extremal values $x^{(2b)}_{\text{ext}}$ is straightforward, but rather lengthy, because it involves higher-order derivatives as well. Thus, we do not present this analysis, since it is not vital for the following. The probability for the extremal $x^{(2b)}_{\text{ext}}$ values is

$$P_\alpha(\chi_\theta|x^{(2b)}_{\text{ext}}) = \frac{1}{\sqrt{2\pi}}e^{-2\{\alpha\cos\theta + [(-1)^n/2]\chi_\theta\}^2}. \tag{39}$$

From the extremal probabilities Eqs. (33), (37), and (39), we find that a conditional probability close to the maximum value can be obtained only if Eq. (30a), or equivalently Eq. (32), is satisfied. A numerical analysis confirms that the implicit Eqs. (30a) or (32) are an excellent approximation for the positions of the maxima of the conditional probability function. A typical example for this is shown in Fig. 3. Therefore, in part of the following, we can simplify our analytical calculations by working with the condition Eq. (32) rather than the full conditional probability Eq. (27).

III. PARTICLE LOCALIZATION

A. One-dimensional localization

To set the stage, we first recover previous results using a single cavity to localize the particle [7]. Suppose the particle flies through a cavity which supports a coherent light field with average photon number $|\alpha|^2$, wave vector k, and

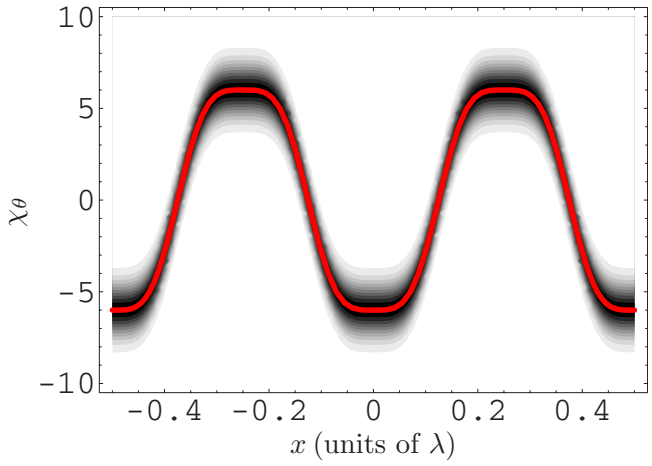

FIG. 3. (Color online) Density plot of the conditional probability $P_\alpha(\chi_\theta|x)$ for $\theta=0$, $\alpha=3$, $\xi=0$. Bright colors indicate low probability, dark colors high probability. The solid (red) line at the center of the dark maximum region indicates the solution to the implicit conditions Eq. (30a) or (32) for the maximum of the probability.

standing-wave phase ξ. The particle imprints a phase shift on the cavity field that can be detected with a quadrature measurement with measurement angle θ and result χ_θ. This allows us to calculate the filter function $P_\alpha(\chi_\theta|x)$ [see Eq. (27)]. Second, one needs to approximately measure the position distribution $|g(x)|^2$ of the particle, e.g., using a lens-based system. The product of the coarse measurement with the filter function then allows one to precisely localize the particle to one of the narrow position peaks given by the filter function. An example of a filter function for a single-phase measurement is shown in Fig. 4. These results are similar to other schemes involving a single measurement reported previously [7].

If the measurement result is χ_θ, then the particle locations with maximum probability are determined by the conditions Eqs. (30a) or (32). Let $x_{\max}$ be a solution to Eq. (32), i.e., a

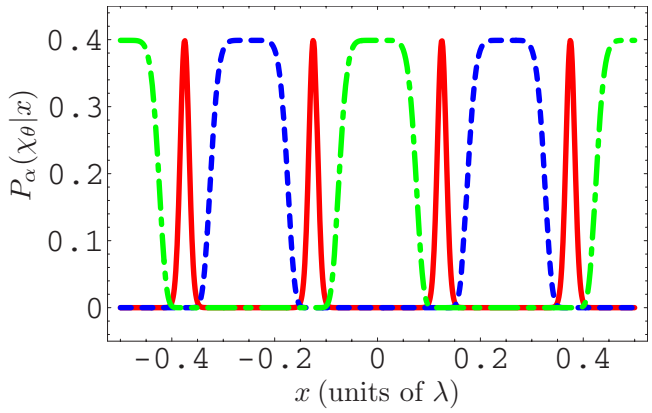

FIG. 4. (Color online) Example filter functions for different results of a single measurement. This corresponds to the probability that a certain value for χ_θ is measured for an actual position x of the quantum particle. The parameters are $\theta=0$, $\alpha=3$, $\xi=0$. The solid (red) line shows the case $\chi_\theta=0$, the dashed (blue) line is for $\chi_\theta=2\alpha$, and the dash-dotted (green) line shows $\chi_\theta=-2\alpha$.

position with maximum probability for the particle localization. From Eq. (32) it follows then that any position $\bar{x}_{\max}$ with $k(\bar{x}_{\max}-x_{\max})=n\pi$, or $(\bar{x}_{\max}-x_{\max})=n\lambda/2$, where n is an integer, is also a solution. This is the usual periodicity of $\cos^2(\cdot)$. Therefore, within a spatial range of one wavelength, several potential positions are possible with maximum probability for a given measurement outcome χ_θ. For example, in Fig. 4, depending on the measurement outcome, two [(blue) dashed curve] or three [dash-dotted (green) curve] wider potential positions or four [solid (red) curve] narrow potential positions are predicted within one wavelength. Therefore, it is in principle desirable to have a conventional coarse measurement of $|g(x)|^2$ with accuracy down to the diffraction limit, which is hard to achieve. Different solutions have been suggested to overcome this limitation by reducing the set of potential positions within one wavelength, for example, to use more complicated level schemes [11].

In the following, we show how several simultaneous particle-cavity interactions with subsequent quadrature measurements can improve the particle localization. Possible setups for one-dimensional particle localization include a single two-mode cavity, or several (near-)parallel cavities that are arranged such that the supported fields overlap at the region in space that the particle flies through. Consider the case of two measurements, giving rise to two different filter functions which both obey Eq. (32) with the respective field parameters. Since the two measurements occur simultaneously, both filter functions must be nonzero at the actual position of the particle. As explained above, however, the filter functions predict potential positions other than the actual position with a certain period in space. But if the spatial period of the two filter functions is different, then for suitable parameters there is only a little overlap between the two filter functions at other positions within one wavelength. Then the product of the two filter functions effectively reduces to at best a single peak per wavelength corresponding to the actual position. An example for such a configuration is shown in Fig. 5. It can be seen that the two individual filter functions shown as dashed (blue) and dash-dotted (green) lines overlap only at certain positions within one wavelength. The solid (red) line in Fig. 5 shows the product of the two conditional probabilities, which corresponds to the filter function for the case of two simultaneous measurements. Figure 5(a) shows the case where the actual position of the particle is around -0.2λ. To create this figure, the parameters for the two fields were fixed, and the measurement outcome for the first field was assumed to be $\chi_{\theta_1}=0$. This allows us to calculate the filter function for the first field. Then it was assumed that, among the potential positions indicated by the first filter function, the peak at around $x=-0.2\lambda$ corresponds to the actual position. A possible measurement outcome for the second field was then evaluated using Eq. (30a) such that also the filter function for the second field has a peak at the actual position of the particle. This fixes the second filter function. The product of the two filter functions now allows one to evaluate the predictive power of the actual measurement. It can be seen that the dual measurement filter function in Fig. 5(a) has a maximum at the actual position $x=-0.2\lambda$, together with two smaller maxima at $x\approx-0.45\lambda$ and $x\approx0.05\lambda$. Thus, the

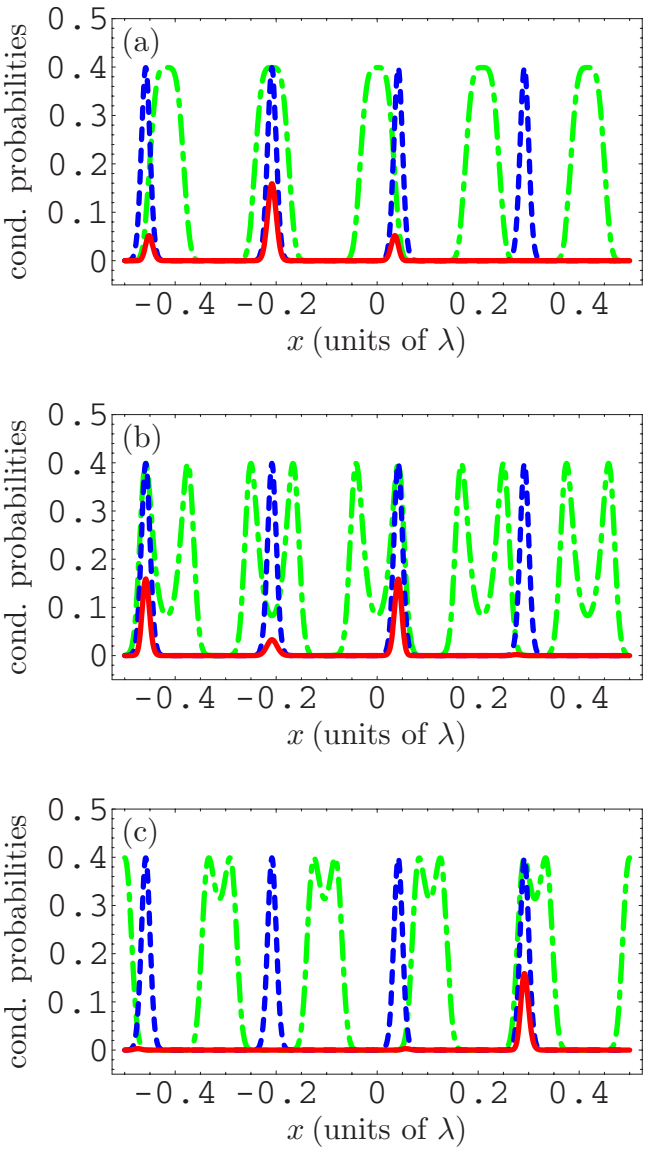

FIG. 5. (Color online) Example filter function for two simultaneous measurements. The dashed (blue) curve shows $P_\alpha(\chi_{\theta_1}|x)$, the dash-dotted (green) line shows $P_\beta(\chi_{\theta_2}|x)$, and the solid (red) line the product $P_\alpha(\chi_{\theta_1}|x)P_\beta(\chi_{\theta_2}|x)$. This product corresponds to the filter function in the dual-measurement case. The parameters for the first field mode are $\theta_1=0$, $\alpha=3$, $\xi_1=\pi/6$, and $\chi_{\theta_1}=0$. The parameters for the second mode are $\theta_2=\pi/2$, $\beta=3$, and $\xi_2=\pi/2$. The wavelength of the second field is chosen smaller than the wavelength λ of the first field by a factor of 1.2. In (a), the measurement outcome χ_{θ_2} for the second mode is chosen consistent with an actual position of the particle at about -0.2λ ($\chi_{\theta_2}\approx 0$). For (b), the position is about 0.05λ ($\chi_{\theta_2}\approx 0.56\pi$), and for (c) it is about 0.3λ ($\chi_{\theta_2}\approx 1.69\pi$).

number of potential positions is only three, as compared to four or five for the two single-mode measurements. In addition, the two-mode measurement maxima are not of equal height; the maxima not corresponding to the actual position are smaller. Thus, the dual measurement considerably improves the localization.

For a meaningful comparison of the predictive power of single and dual measurements, different positions of the particle need to be considered for the same field parameters. The reason for this is that, in the actual experiment, the field parameters have to be chosen without knowledge of the actual position of the particle. Thus, Figs. 5(b) and 5(c) show results for the same field mode parameters as in Fig. 5(a), but for different actual positions of the particle. In Fig. 5(b), again the number of potential positions predicted from the measurement is reduced to three. In this case, however, two peaks of approximately equal height are present, one of which corresponds to the actual position at about $x=0.05\lambda$. The third peak is much smaller. In Fig. 5(c), the actual position is at about $x=0.3\lambda$. Here, near-perfect results are obtained from the dual measurement. The filter function reduces to a single narrow peak located at the true particle position. This would allow us to unambiguously locate the particle within the region of a wavelength.

If the dual measurement reduces the set of potential positions, then the desired accuracy of the additional conventional measurement is reduced, thus relaxing the experimental requirements. For example, in Fig. 5(c), an accuracy of $\sim\lambda$ is sufficient to localize the particle to a single narrow position in space with width well below $\lambda/10$, as indicated by the solid (red) line. Note that, independent of the number of phase shift measurements, for each spatial dimension only a single conventional measurement is required, but with different accuracy depending on the number of phase shift measurements.

B. Multidimensional localization

The generalization of the above considerations for the localization in more than one spatial dimension is straightforward. Different cases can be distinguished. For example, two cavities orthogonal to each other could be used to measure the position in two spatial dimensions with a single quadrature measurement per direction. This setup is shown in Fig. 2. No additional theoretical considerations are required, since the two measurements are independent. Additionally, the localization in each of the directions can be improved by applying several simultaneous measurements in a single direction (for example by using a multimode cavity), as discussed in Sec. III A. Note that also for multiple independent quadrature measurements only a single conventional measurement is required per direction. Similarly, the localization can also be extended to all three spatial dimensions.

IV. WAVE-FUNCTION MEASUREMENT

In previous work, it was shown that atomic center-of-mass (c.m.) wave-function measurement is possible using schemes similar to atom localization setups [20]. Despite the similar setup, this type of measurement is rather different from the localization described so far. In order to explain this and to discuss why simultaneous measurements as discussed in this paper allow one to improve wave-function measurements, we need to discuss in detail how localization schemes enable one to measure a wave function. For simplicity, we start with the case of a single quadrature measurement. From Eqs. (24) and (27), we find in this case

$$P(x|\chi_\theta^\alpha) = N^2 |g(x)|^2 P_\alpha(\chi_\theta^\alpha|x). \quad (40)$$

In the particle localization discussed so far, the aim is to obtain $P(x|\chi_\theta^\alpha)$, that is, to obtain the precise position of the particle flying through the measurement apparatus. For this, the field quadrature is measured in order to evaluate $P_\alpha(\chi_\theta^\alpha|x)$, and a coarse-grained measurement of the particle position with accuracy within the fundamental limitations yields $|g(x)|^2$. Thus, here the filter function $P_\alpha(\chi_\theta^\alpha|x)$ allows one to boost the accuracy of the measurement of $|g(x)|^2$.

In the wave-function measurement, however, both $P(x|\chi_\theta^\alpha)$ and $P_\alpha(\chi_\theta^\alpha|x)$ are directly measured in the experiment, with the aim of extracting $g(x)$, i.e., both the amplitude and phase of the c.m. wave function.

To show how the filter function allows us to improve the wave-function measurement, consider first the case without this additional measurement. Then, $P(x)=|g(x)|^2$. Thus, a direct measurement does give information on the wave-function modulus, but only up to the fundamental limitations of a position measurement such as the diffraction limit. We now turn to the case with the additional quadrature measurement, and proceed by approximating $P_\alpha(\chi_\theta^\alpha|x)$ by its maximum probabilities as discussed in Sec. II D. Then the function $P_\alpha(\chi_\theta^\alpha|x)$ is characterized by Eq. (32), and we define the set of positions x that satisfy Eq. (32) for a given measurement outcome χ as $\mathcal{M}(\chi)$. Then Eq. (40) can be written as

$$P(x|\chi_\theta^\alpha) = \bar{N}^2 \sum_{y\in\mathcal{M}(\chi_\theta^\alpha)} |g(y)|^2 \delta(x-y), \quad (41)$$

where the normalization $\bar{N}$ follows from N by incorporating the maximum amplitude of the filter function, and $\delta(\cdot)$ is the Kronecker delta function. This approximation is rather good if the measurement outcome χ_θ^α is close to 0, but becomes worse if $|\chi_\theta^\alpha|$ approaches its maximum possible value. This can be seen from Fig. 3. For example, in this figure a horizontal cut at $\chi_\theta^\alpha=0$ yields a set of four small intersection regions with the conditional probability, and thus a well-defined set $\mathcal{M}(\chi_\theta^\alpha)$. For $\chi_\theta^\alpha=6$, however, the intersection consists of two rather wide regions around $x=\pm 0.25$. In this case, the choice of $\mathcal{M}(\chi_\theta^\alpha)$ cannot be made accurately. In an experiment, this problem can be avoided by dropping measurements with large values of χ_θ^α from the analysis.

Thus, the field quadrature measurement implies via the filter function that the particle can only be at specific positions given by the filter function. Thus, the typically smooth and continuous c.m. wave-function distribution is reduced to a discrete set of potential positions. Then, even if the position measurement accuracy is limited, the measured position can be attributed to a rather precise position out of the set of potential positions given by the filter function. This enables one to directly extract $|g(x)|$ at this particular position in space. A series of measurements with different field configurations and thus different filter functions then allows reconstruction of the full wave-function modulus $|g(x)|$ for all values of x.

For this scheme to work successfully, the position measurement should have a resolution that exceeds the distance of the individual peaks of the filter function. Since a filter function obtained via a single measurement in general has several potential positions per wavelength, this is rather challenging. Several simultaneous measurements allow reduction of the number of potential positions per wavelength as shown in Sec. III A, and thus relax the required resolution of the position measurement. It is in this sense that multiple simultaneous quadrature measurements can improve the wave-function measurement.

To completely determine the wave function, also the phase information of $g(x)$ needs to be recovered. In contrast to the modulus $|g(x)|$, this is not possible using a simple position detector. It was shown in previous work, however, that a localization scheme also allows one to obtain the phase information to recover the full wave function [20]. For this, we consider the projection of the wave function Eq. (22) after the particle has passed the standing-wave fields on momentum eigenstates $|p\rangle$ and electronic ground state $|g\rangle$, using the relation $\langle p|x\rangle=(2\pi\hbar)^{-1/2}\exp(-ipx/\hbar)$. We obtain

$$\begin{aligned}\langle p,g|\Psi(t)\rangle &= N\int dx\, g(x)\langle\chi_{\theta_1}^\alpha|\alpha e^{i\phi_1 t}\rangle\langle\chi_{\theta_2}^\beta|\beta e^{i\phi_2 t}\rangle\langle\chi_{\theta_3}^\gamma|\gamma e^{i\phi_3 t}\rangle \\ &\quad\times\langle p,g|x,g\rangle \\ &= \frac{N}{\sqrt{2\pi\hbar}}\int dx\, g(x)A(\chi_{\theta_1}^\alpha,\chi_{\theta_2}^\beta,\chi_{\theta_3}^\gamma,x)e^{-(i/\hbar)px}, \quad (42)\end{aligned}$$

where we have defined, using Eq. (26),

$$\begin{aligned}A(\chi_{\theta_1}^\alpha,\chi_{\theta_2}^\beta,\chi_{\theta_3}^\gamma,x) &= \langle\chi_{\theta_1}^\alpha|\alpha e^{i\phi_1 t}\rangle\langle\chi_{\theta_2}^\beta|\beta e^{i\phi_2 t}\rangle\langle\chi_{\theta_3}^\gamma|\gamma e^{i\phi_3 t}\rangle \\ &= A_\alpha(\chi_{\theta_1}^\alpha,x)A_\beta(\chi_{\theta_2}^\beta,x)A_\gamma(\chi_{\theta_3}^\gamma,x).\end{aligned}$$

Note that $A_\alpha(\chi_{\theta_1}^\alpha,\chi_{\theta_2}^\beta,\chi_{\theta_3}^\gamma,x)$ is the amplitude corresponding to the combined filter function arising from three simultaneous measurements. From this, the conditional momentum probability follows as

$$\begin{aligned}&P(p,\chi_{\theta_1}^\alpha,\chi_{\theta_2}^\beta,\chi_{\theta_3}^\gamma) \\ &= |\langle p,g|\Psi\rangle|^2 = \frac{|N|^2}{2\pi\hbar}\left|\int dx\, g(x)A(\chi_{\theta_1}^\alpha,\chi_{\theta_2}^\beta,\chi_{\theta_3}^\gamma,x)e^{-(i/\hbar)px}\right|^2 \\ &= \frac{|\hat{N}|^2}{2\pi\hbar}\left|\int dx\sum_{y\in\mathcal{M}} g(x)A(\chi_{\theta_1}^\alpha,\chi_{\theta_2}^\beta,\chi_{\theta_3}^\gamma,y)\right. \\ &\quad\left.\times\delta(x-y)e^{-(i/\hbar)px}\right|^2 \\ &= \frac{|\tilde{N}|^2}{2\pi\hbar}\left|\sum_{y\in\mathcal{M}}|g(y)|A(\chi_{\theta_1}^\alpha,\chi_{\theta_2}^\beta,\chi_{\theta_3}^\gamma,y)e^{i\rho(y)-(i/\hbar)py}\right|^2. \quad (43)\end{aligned}$$

We again have approximated the filter function by a set of discrete points $\mathcal{M}=\mathcal{M}(\chi_{\theta_1}^\alpha,\chi_{\theta_2}^\beta,\chi_{\theta_3}^\gamma)$, similar to the case in Eq. (41), and N, $\hat{N}$, and $\tilde{N}$ are normalization constants. One difference, however, is that Eq. (43) depends on the amplitude $A(\chi_{\theta_1}^\alpha,\chi_{\theta_2}^\beta,\chi_{\theta_3}^\gamma,x)$ rather than the probability $P_\alpha(\chi_{\theta_1}^\alpha|x)P_\beta(\chi_{\theta_2}^\beta|x)P_\gamma(\chi_{\theta_3}^\gamma|x)$ as in Eq. (41). Therefore, here we have replaced

$$A(\chi^{\alpha}_{\theta_1},\chi^{\beta}_{\theta_2},\chi^{\gamma}_{\theta_3},x) \to \frac{\bar{N}}{N}\sum_{y\in\mathcal{M}} A(\chi^{\alpha}_{\theta_1},\chi^{\beta}_{\theta_2},\chi^{\gamma}_{\theta_3},y)\,\delta(x-y), \tag{44}$$

where the fraction $\bar{N}/N$ corresponds to the normalization change due to the introduction of the Kronecker delta function. This extended replacement is required since the amplitude $A(\chi^{\alpha}_{\theta_1},\chi^{\beta}_{\theta_2},\chi^{\gamma}_{\theta_3},x)$ contains phase information, unlike the probability in Eq. (41). Further, we have defined $g(x)=|g(x)|\exp[i\rho(x)]$. A measurement of the conditional probability distribution $P(p,\chi^{\alpha}_{\theta_1},\chi^{\beta}_{\theta_2},\chi^{\gamma}_{\theta_3})$, together with measurements on the field states thus in principle, give all entities occurring in Eq. (43) but the desired phase $\rho(x)$. As discussed in [20], a sample of measurements with different field configurations yields a set of equations of the type of Eq. (43), which can be solved for the phase difference between adjacent points in the set $\mathcal{M}$. Since the overall phase of the c.m. wave function is irrelevant, this suffices to recover the phase information of the wave function approximately.

After this brief outline of the method, we now turn to a discussion of how multiple simultaneous measurements can improve this scheme. Similar to the measurement of the modulus, an identification of a discrete set of potential positions $\mathcal{M}$ via the filter function is the key to the wave-function phase measurement. Simultaneous measurements allow us to reduce the number of potential positions, i.e., to minimize the set $\mathcal{M}$. This in turn lessens the experimental and computational complexity, and therefore improves the phase measurement.

In addition to the one-dimensional wave-function recovery discussed so far, obviously a multidimensional localization measurement (see Sec. III B) also allows one to obtain the c.m. wave functions in more than one dimension simultaneously.

V. DISCUSSION AND SUMMARY

We have discussed particle localization and wave-function measurements using several simultaneous field quadrature measurements of independent cavity modes. The measurement of the different cavity mode quadratures reveals the phase shift that is imprinted on the cavity fields due to a dispersive interaction with the particle during its flight through the cavity fields.

Thus, the setup consists of two parts. The first part involves the simultaneous passage of the atom through standing-wave fields. Several experiments of this type have been performed with a single mode, both in the Raman-Nath [21] and in the Bragg deflection regime [22]. Our scheme requires an extension either to multimode cavities or to several perpendicular cavity fields in order to allow for simultaneous measurements. Ideally, the frequencies of the different modes should be different, but since we consider dispersive interaction, the cavity fields do not need to be in resonance with the different atomic transitions, which simplifies the use of multimode cavities. The second part is the detection of the phase shifts imprinted on the cavity fields. Measurements of these type are common, e.g., in entanglement detection, and can be realized via homodyne detection [23]. In [9], two possible schemes are suggested. Either Q switching of the cavity field could be used to extract the cavity field to the detection system after the atom has passed, or the cavity could be placed in one arm of an interferometer such that phase shifts due to the passage of the atom could be measured via a change of the interference pattern. For the Q-switching case, the different cavities could be measured one after another using the same detector if the Q switching is applied sequentially to the different cavity fields. It may also be possible to measure the different phases simultaneously using setups as required for the detection of squeezed light [24].

In general, measurements such as the field quadrature determination give rise to so-called filter functions. These filter functions can be used to refine a conventional position measurement to a localization of the particle to a few potential subwavelength regions in space. We have shown that several simultaneous measurements give rise to an improved filter function, which allows us to relax the requirements for the classical coarse position measurement, and to reduce the number of potential subwavelength localization regions. Similar improvement is possible for the measurement of the center-of-mass wave function of the particle. Also in this case, we have shown that an improved filter function can be obtained that relaxes the conditions on the required measurements. In addition to the improvement of the measurements in one spatial dimension, multiple measurements can also be used to localize or to measure the wave function in two or even three spatial dimensions.

ACKNOWLEDGMENTS

The authors thank COMSTECH for their support. J.E. gratefully acknowledges hospitality at the Center for Quantum Physics (CIIT), Islamabad, Pakistan.

[1] S. W. Hell, Nat. Biotechnol. **21**, 1347 (2003); U. W. Rathe and M. O. Scully, Lett. Math. Phys. **34**, 297 (1995); A. N. Boto, P. Kok, D. S. Abrams, S. L. Braunstein, C. P. Williams, and J. P. Dowling, Phys. Rev. Lett. **85**, 2733 (2000); M. D'Angelo, M. V. Chekhova, and Y. Shih, *ibid.* **87**, 013602 (2001); A. Muthukrishnan, M. O. Scully, and M. S. Zubairy, J. Opt. B: Quantum Semiclassical Opt. **6**, S575 (2004); W. Denk, J. H. Strickler, and W. W. Webb, Science **248**, 73 (1990).

[2] A. Lewis, M. Isaacson, A. Harootunian, and A. Muray, Ultramicroscopy **13**, 227 (1984); A. Lewis, H. Taha, A. Strinkovski, A. Manevitch, A. Khatchatouriants, R. Dekhter, and E. Ammann, Nat. Biotechnol. **21**, 1378 (2003).

[3] S. Hell and E. H. K. Stelzer, J. Opt. Soc. Am. A **9**, 2159 (1992).

[4] S. W. Hell and J. Wichmann, Opt. Lett. **19**, 780 (1992); T. A. Klar, S. Jakobs, M. Dyba, A. Egner, and S. W. Hell, Proc. Natl. Acad. Sci. U.S.A. **97**, 8206 (2000).

[5] F. LeKien, G. Rempe, W. P. Schleich, and M. S. Zubairy, Phys. Rev. A **56**, 2972 (1997).

[6] S. Qamar, S.-Y. Zhu, and M. S. Zubairy, Phys. Rev. A **61**, 063806 (2000); S. Qamar, S.-Y. Zhu, and M. S. Zubairy, Opt. Commun. **176**, 409 (2000); F. Ghafoor, S. Qamar, and M. S. Zubairy, Phys. Rev. A **65**, 043819 (2002); T. Azim, M. Ikram, and M. S. Zubairy, J. Opt. B: Quantum Semiclassical Opt. **6**, 248 (2004); D.-c. Cheng, Y.-p. Niu, R.-x. Li, and S.-q. Gong, J. Opt. Soc. Am. B **23**, 2180 (2006).

[7] P. Storey, M. Collett, and D. Walls, Phys. Rev. Lett. **68**, 472 (1992); Phys. Rev. A **47**, 405 (1993).

[8] R. Quadt, M. Collett, and D. F. Walls, Phys. Rev. Lett. **74**, 351 (1995).

[9] M. A. M. Marte and P. Zoller, Appl. Phys. B: Photophys. Laser Chem. **54**, 477 (1992).

[10] A. M. Herkommer, H. J. Carmichael, and W. P. Schleich, Quantum Semiclassic. Opt. **8**, 189 (1996).

[11] M. Sahrai, H. Tajalli, K. T. Kapale, and M. S. Zubairy, Phys. Rev. A **72**, 013820 (2005); K. T. Kapale and M. S. Zubairy, *ibid.* **73**, 023813 (2006).

[12] H. Nha, J.-H. Lee, J.-S. Chang, and K. An, Phys. Rev. A **65**, 033827 (2002).

[13] M. Macovei, J. Evers, C. H. Keitel, and M. S. Zubairy, Phys. Rev. A **75**, 033801 (2007).

[14] M. O. Scully and M. S. Zubairy, *Quantum Optics* (Cambridge University Press, Cambridge, U.K., 1997).

[15] Z. Ficek and S. Swain, *Quantum Interference and Coherence: Theory and Experiments* (Springer, Berlin, 2005).

[16] C. Cohen-Tannoudji, J. Dupont-Roc, and G. Grynberg, *Atom-Photon Interactions: Basic Processes and Applications* (Wiley-VCH, Berlin, 1998).

[17] C. J. Villas-Bôas, N. G. de Almeida, R. M. Serra, and M. H. Y. Moussa, Phys. Rev. A **68**, 061801(R) (2003).

[18] R. R. Puri and R. K. Bullough, J. Opt. Soc. Am. B **5**, 2021 (1988).

[19] M. Alexanian and S. K. Bose, Phys. Rev. A **52**, 2218 (1995); Y. Wu, *ibid.* **54**, 1586 (1996).

[20] K. T. Kapale, S. Qamar, and M. S. Zubairy, Phys. Rev. A **67**, 023805 (2003).

[21] P. J. Martin, P. L. Gould, B. G. Oldaker, A. H. Miklich, and D. E. Pritchard, Phys. Rev. A **36**, 2495 (1987); C. Kurtsiefer, T. Pfau, C. R. Ekstrom, and J. Mlynek, Appl. Phys. B: Lasers Opt. **60**, 229 (1995); S. Kunze, S. Dürr, K. Dieckmann, M. Elbs, U. Ernst, A. Hardell, S. Wolf, and G. Rempe, J. Mod. Opt. **44**, 1863 (1997).

[22] P. J. Martin, B. G. Oldaker, A. H. Miklich, and D. E. Pritchard, Phys. Rev. Lett. **60**, 515 (1988); D. M. Giltner, R. W. McGowan, and S. A. Lee, Phys. Rev. A **52**, 3966 (1995); S. Kunze, S. Dürr, and G. Rempe, Europhys. Lett. **34**, 343 (1996); S. Dürr, S. Kunze, and G. Rempe, Quantum Semiclassic. Opt. **8**, 531 (1996); M. K. Oberthaler, R. Abfalterer, S. Bernet, J. Schmiedmayer, and A. Zeilinger, Phys. Rev. Lett. **77**, 4980 (1996).

[23] O. Glöckl, U. L. Andersen, and G. Leuchs, Phys. Rev. A **73**, 012306 (2006).

[24] A. M. Marino, C. R. Stroud, Jr., V. Wong, R. S. Bennink, and R. W. Boyd, J. Opt. Soc. Am. B **24**, 335 (2007).